Available online at www.sciencedirect.com

SciVerse ScienceDirect

Energy Procedia 37 (2013) 370 – 385

Energy Procedia

GHGT-11

Absorption rates and CO_2 solubility in new piperazine blends

Le Li[a], Han Li[b], Omkar Namjoshi [a], Yang Du[a], Gary T. Rochelle[a]*

[a] *The University of Texas at Austin, Department of Chemical Engineering. Luminant Carbon Management Program, 200 E Dean Keeton St. Stop C0400, Austin, TX 78712-1589*

[b] *State Key Laboratory of Chemical Engineering ,Tsinghua University, Beijing 100084, China*

Abstract

The absorption rate and CO_2 solubility of four new blends using concentrated piperazine (PZ) were measured. The blends are 6 m PZ/2 m hexamethylenediamine (HMDA), 6 m PZ/2 m diaminobutane (DAB), 6 m PZ/2 m bis(aminoethyl)ether (BAE), and 5 m PZ/2 m N-2(aminoethy)lpiperazine (AEP). The liquid film mass transfer coefficient (k_g') of the blends was measured at 20–100 °C using a wetted wall column (WWC). P_{CO2}* was measured at 20–100 °C using the WWC, and at 100–160 °C using a total pressure apparatus. A semi-empirical VLE model was regressed for each blend using measured P_{CO2}*, and the models show good agreement with experimental data. The process performance of the new blends is compared to 5 m PZ/2.3 m AMP, 2 m PZ/4 m AMP, 8 m PZ, and 7 m MEA. The high pKa of primary diamines contributes to high lean and rich loading and low solvent capacity for 6 m PZ/2 m HMDA, 6 m PZ/2 m DAB, 6 m PZ/2 m BAE. The ΔH_{abs} of PZ/AEP and PZ/AMP is competitive with 7 m MEA. PZ/BAE and PZ/HMDA have ΔH_{abs} higher than 8 m PZ but lower than 7 m MEA. The energy performance of the solvent depends on CO_2 VLE and thermal stability. 6 m PZ/2 m HMDA, 6 m PZ/2 m AEP, and 5 m PZ/2 m BAE show good energy performance and are competitive with 8 m PZ. At 40 °C the absorption rate of 5 m PZ/2 m AEP is about the same as 8 m PZ; 6 m PZ/2 m DAB and 6 m PZ/2 m BAE have 10% lower rates than 8 m PZ.

Selection and/or peer-review under responsibility of GHGT

Keywords: Piperazine; Solvent blends; Absorption rate; CO_2 solubility; Capacity; Energy performance

1. Introduction

This work presents absorption rate and CO_2 solubility measurements for new PZ blends with high PZ concentration (25–30 wt %). The blends are 6 m PZ/2 m hexamethylenediamine (HMDA), 6 m PZ/2 m diaminobutane (DAB), 6 m PZ/2 m bis(aminoethyl)ether (BAE), and 5 m PZ/2 m N-

* Corresponding author. Tel.: +1-512-471-7230; fax: +1-512-475-7824.
E-mail address: gtr@che.utexas.edu.

1876-6102
Selection and/or peer-review under responsibility of GHGT
doi:10.1016/j.egypro.2013.05.122

2(aminoethy)lpiperazine (AEP). All four amines have high alkalinity per molecule, which provides higher CO_2 carrying capacity (mol N/kg amine). The HMDA and BAE blends are expected to have high thermal stability [1]. The volatility of all four blends should have similar volatility to 8 m PZ due to the low concentration of the other amine. Results of the blends are compared against two PZ blends using 2-amino-2-methyl-1propanol (AMP): 5 m PZ/2.3 m AMP and 2 m PZ 4 m AMP [2]. The molecular structures of the amines are show in Table 1. All of the PZ blends are also compared against 8 m PZ and 7 m MEA [3,4].

Table 1: Molecular structure of amines used in new PZ blends

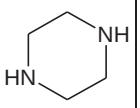 Piperazine (PZ)	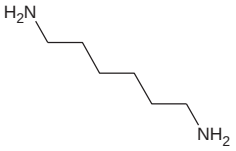 Hexamethylenediamine (HMDA)	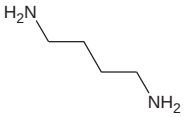 Diaminobutane (DAB)	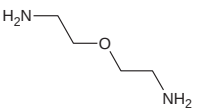 Bis(aminoethyl)ether (BAE)	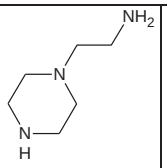 N-2(aminoethyl) piprazine (AEP)	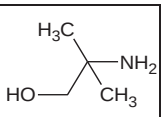 2-amino-2-methyl-1propanol (AMP)

1.1. CO_2 solubility

The CO_2 solubility can be used to predict the overall energy performance and the operating loading range of the solvent. Process modeling results for coal-fired flue gas show 8 m PZ to have the best overall energy performance when operating between P_{CO2}* at 0.5 and 5 kPa at the top and bottom of the absorber [6]. Thus, the nominal lean and rich conditions of a solvent are defined as the CO_2 loading that corresponds to these P_{CO2}* at 40 °C. Solvent performance is compared at this practical loading range.

1.2. Absorption rate

Solvents with high absorption rate require less packing while removing the same amount of CO_2, which means lower capital cost for the process. Also, a high absorption rate can reduce the driving force for mass transfer in the absorber and the overall irreversibility of the process [5]. This reduces the overall energy cost.

Absorption rate is measured by a bench scale wetted wall column (WWC). The liquid film mass transfer coefficient (k_g') is reported, which equals the CO_2 flux divided by the liquid side driving force expressed using CO_2 partial pressure (Equation 1).

$$k_g' = \frac{CO_2\ flux}{(P_{CO_2,interface} - P^*_{CO_2,bulk\ solution})} \quad (1)$$

k_g' depends on intrinsic solvent properties and the hydrodynamics of the gas-liquid contactor. Since the hydrodynamic of the WWC is relatively constant among solvents, the difference in measured k_g' represents changes in solvent properties. Thus, the WWC is superior to alternative methods, particularly gas sparging, where the contactor hydrodynamics can vary significantly due to changes in the physical properties of solvents. Also, compared to the stirred cell and the laminar jet, mass transfer in the WWC is more similar to that in structured packing. Results measured by the WWC can be used directly to predict solvent performance with commercial packing.

For most practical absorption conditions, the pseudo first order (PFO) approximation can be applied to the reaction between CO_2 and amines, which assumes the concentration of free amine in the boundary layer is the same as the bulk liquid. When this assumption is valid, k_g' has a simplified expression as shown in Equation 2.

$$k'_g \approx \frac{\sqrt{D_{CO_2} k_2 [Amine]_b}}{H_{CO_2}} \quad (2)$$

The PFO expression shows k_g' is a function of diffusivity of CO_2 in the liquid (D_{CO2}), the reaction rate constant of CO_2 and the amine (k_2), the free amine concentration in the bulk solution, and the Henry's constant of CO_2 over the solvent (H_{CO2}). Thus, the reaction rate constant (k_2) alone cannot be used to represent the practical absorption rate. Also, absorption rate should be measured at practical amine concentration and CO_2 loading, because the free amine concentration can vary significantly with changes in loading.

2. Experimental methods

2.1. Wetted wall column

The detailed geometry of the wetted wall column is shown in Figure 1. This WWC and experimental method are identical to those used by Chen [7, 8], and Dugas [3]. The total gas-liquid contact area of the column is calculated to be 38.5 cm^2 for ideal liquid film. The hydraulic diameter of the contact chamber is 0.44 cm, and 1.3 cm^2 cross area for gas flow. During an experiment, liquid solvent is pumped from a 1 liter reservoir and circulated through the WWC in a closed loop at approximately 2.4 $X10^{-4}$ standard m^3/min. The solvent enters the chamber through the hollow center of the column, and falls downward along its outer wall, forming an evenly distributed film, then exits from the bottom of the contact chamber. A total gas flow of 5 $X10^{-3}$ standard m^3/min is prepared by mixing CO_2 with N_2. The gas stream is first saturated with water prior to entering the bottom of the contact chamber. The exit gas leaves from the top of the chamber. The CO_2 in the gas is measured by a Horiba Infrared Detector before and after entering the chamber. The total pressure of the system is varied between 0.5 MPa and 0.7 MPa, which is controlled by a needle valve at the gas exit. The gas and liquid streams both pass through temperature-controlled oil baths, which also set the temperature of the oil jacket of the chamber.

The difference in gas phase CO_2 concentration before and after entering the chamber is used to calculate the CO_2 flux of absorption/desorption. Typically, six measurements with different inlet CO_2 partial pressures are made for one CO_2 loading and temperature by varying the CO_2/N_2 ratio in the gas. The CO_2 partial pressure is chosen between zero and double the equilibrium partial pressure of the solvent (P_{CO2}*); with three higher than P_{CO2}*for absorption and three lower for desorption. The measured CO_2 flux should form a straight line when plotted against the partial pressure driving force, as described by Equation 3.

$$CO_2\ flux = K_G (P_{CO_2,g} - P^*_{CO_2})_{LM} \quad (3)$$

While the value for P_{CO2}* is unknown, it is calculated by trial and error until Equation 3 satisfies the condition where CO_2 flux is zero when the driving force is zero. The linear function of the measured points should pass through the original point with the correct P_{CO2}* (Figure 2). The slope of the line is the overall gas side mass transfer coefficient (K_G). k_g' is calculated by subtracting the gas film resistance ($1/k_g$) from the overall resistance (Equation 4). The gas film mass transfer coefficient (k_g) is calculated using an empirical correlation previously characterized for this wetted wall column [9].

$$\frac{1}{k'_g} = \frac{1}{K_G} - \frac{1}{k_g} \quad (4)$$

The WWC is used to measure k_g' and P_{CO2}* for each solvent at 20–100 °C and variable CO_2 loading.

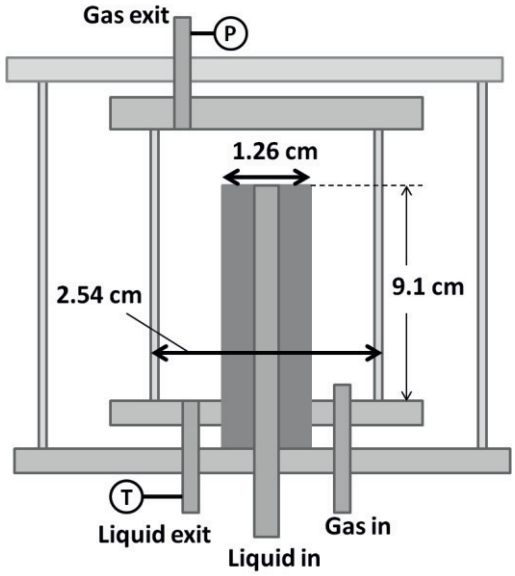

Figure 1: Detailed wetted wall column dimensions

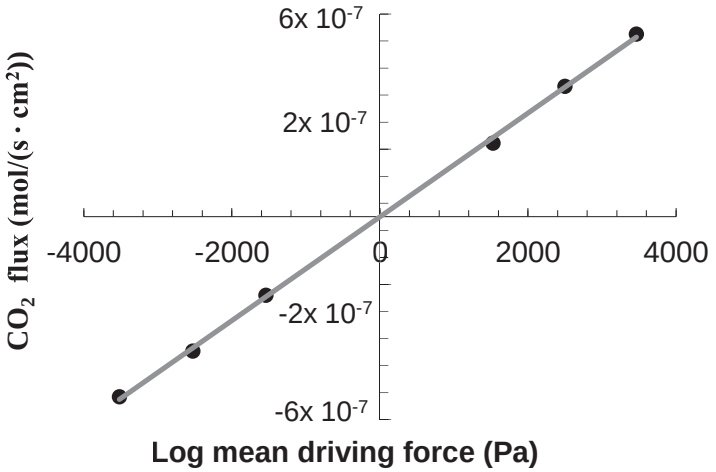

Figure 2: Experimental CO_2 flux and partial pressure driving force measured for 5 m PZ/2m AEP with 0.25 mol/mol alk CO_2 loading at 80 °C

2.2. Total pressure

A total pressure equilibrium reactor is used to measure CO_2 partial pressure at high temperature. The experimental apparatus and procedure are identical to those used by Xu [4].

During an experiment, approximately 350 mL of liquid solvent with CO_2 loading is placed in the 500 mL equilibrium reactor. The head space of the reactor is flushed with N_2 before the reactor is sealed.

The pressure of the reactor is measured continuously as it is heated to target temperatures. The reactor is kept at each temperature for at least 20 minutes after the reactor temperature stabilizes in order to ensure equilibrium is reached. The P_{CO2}^* at each temperature is calculated from the measured reactor pressure (P_{meas}) using Equation 5.

$$P_{CO_2}^* = P_{meas} - P_{N_2} - P_{H_2O} - P_{amine} = P_{meas} - T \cdot \frac{P_{N_2\,initial}}{T_{initial}} - P_{H_2O,vap} \cdot x_{H_2O} \quad (5)$$

The ideal gas law is assumed where the total system pressure equals the sum of the partial pressure of its components. The partial pressure of nitrogen (P_{N2}) is approximated using the ideal gas law and the initial reactor temperature and pressure. The partial pressure of water is calculated using Raoult's law. Literature value from the DIPPR database is used for the vapour pressure of water ($P_{H2O,Vap}$) [10]. The partial pressure of the amine (P_{amine}) is assumed to be zero since it is expected to be negligible compared to the partial pressure of other species.

CO_2 loading of the initial solvent and at the end of the experiment is measured. However, the CO_2 loading at each temperature is expected to change significantly from the initial condition due to the high CO_2 partial pressure. Therefore, the CO_2 loading values are corrected by subtracting the moles of CO_2 in the vapor phase (n_{CO_2V}) from total CO_2 in the original sample (n_{CO_2T}) as in Equation 6.

$$\propto = \frac{n_{CO_2T} - n_{CO_2V}}{n_{alkalinity}} = \frac{n_{CO_2T} - \frac{P_{CO_2V}Vvap}{RT}}{n_{alkalinity}} \quad (6)$$

The vapor phase CO_2 (n_{CO_2V}) is calculated using the ideal gas law, where V_{vap} is the vapor volume of the equilibrium reactor (approx 150 mL).

The total pressure apparatus can operate from 100 to 160 °C, and measures P_{CO2}* accurately in the range of 0.1–2.0 MPa.

2.3. Analytical methods

The CO_2 loading in the liquid solvent is determined by the total inorganic carbon method and acid titration. The total inorganic carbon method measures the amount of CO_2 per unit mass of liquid sample. The acid titration method measures the total moles of equivalent alkalinity per unit mass of solvent. Both methods are identical to those described by Freeman [11].

HMDA (Acros, 99%), DAB (Acros, 99%), BAE (Huntsman, 99%), AEP (Acros, 99%), and PZ (Sigma-Aldridge, 98%) are used to prepare the solvents. CO_2 loading in the liquid are generated by bubbling gaseous CO_2 (99.99%, Matheson Tri-Gas) into the solvent.

3. Results and discussion

Experimental results for k_g' and P_{CO2}* are tabulated in Tables 4–6.

3.1. CO_2 solubility

About 20–50 data points were collected for each blend at variable CO_2 loading across the nominal lean and rich loading range using the WWC and total pressure apparatus. For each solvent, a semi-empirical VLE model is developed by regression of all experimental data using Equation 7.

$$\ln\left(P_{CO_2}^*\right) = a + \frac{b}{T} + c \cdot \alpha + d \cdot \alpha^2 + d\frac{\alpha}{T} + e\frac{\alpha^2}{T} \quad (7)$$

The values of model parameters and their statistical significance are summarized in Table 2. The quality of the regressed fit by the model (R^2) is included. The experimental results are plotted together with model predictions for the blend in Figures 3–5.

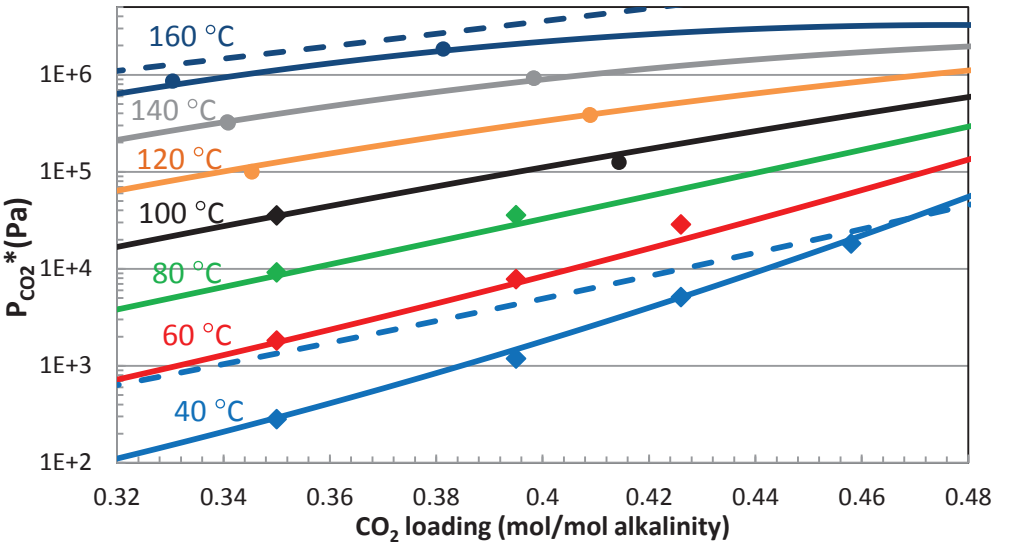

Figure 3: CO_2 solubility in 6 m PZ/2 m HMDA. Diamonds: WWC results; Circles: total pressure results; Solid lines: model prediction (Equation 7); Dashed lines: model for 8 m PZ [4].

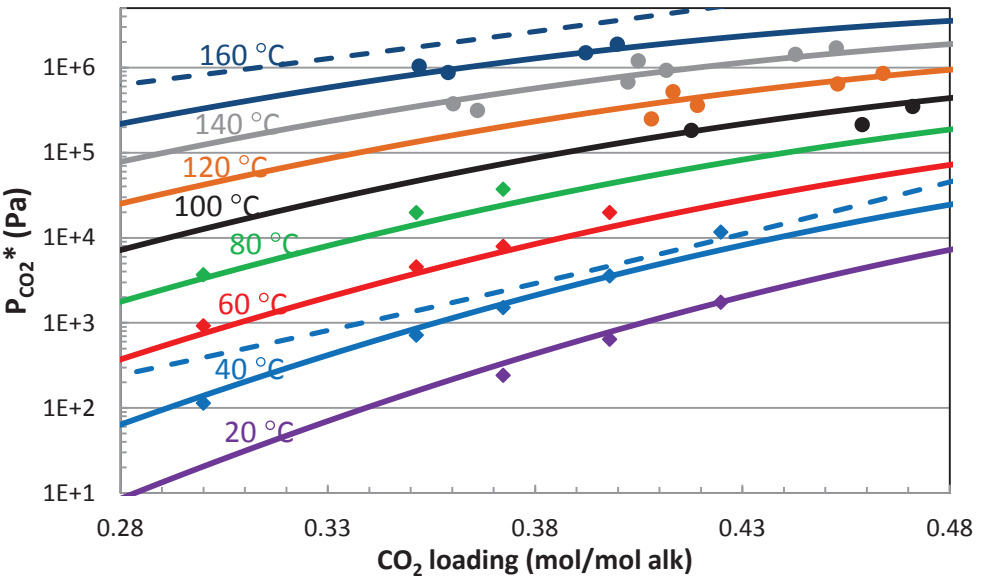

Figure 4: CO_2 solubility in 6 m PZ/2 m DAB. Diamonds: WWC results; Circles: total pressure results; Solid lines: model prediction (Equation 7); Dashed lines: model for 8 m [4].

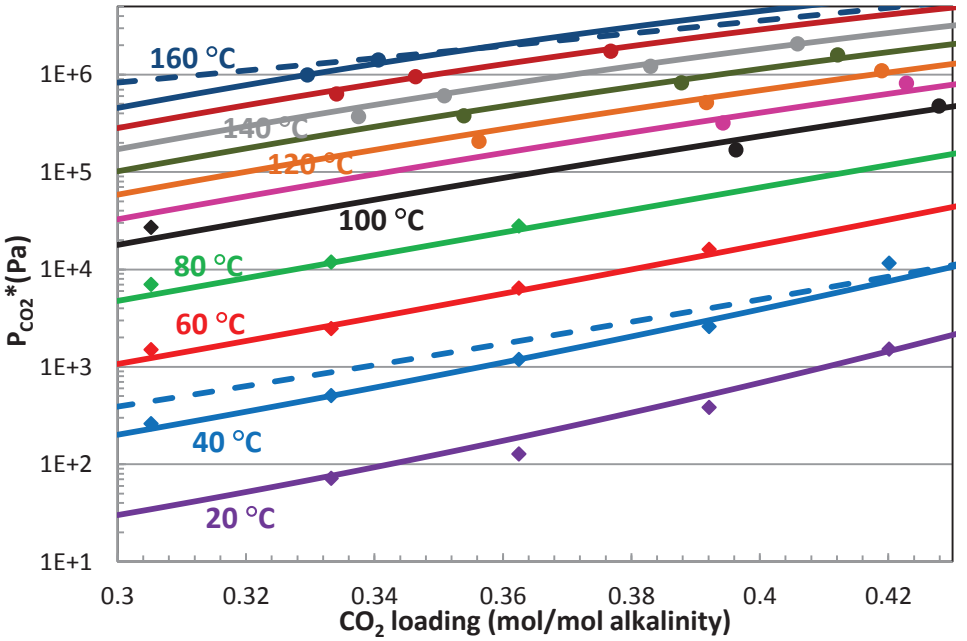

Figure 5: CO_2 solubility in 6 m PZ/2 m BAE. Diamonds: WWC results; Circles: total pressure results; Solid lines: model prediction (Equation 7); Dashed lines: model for 8 m PZ [4].

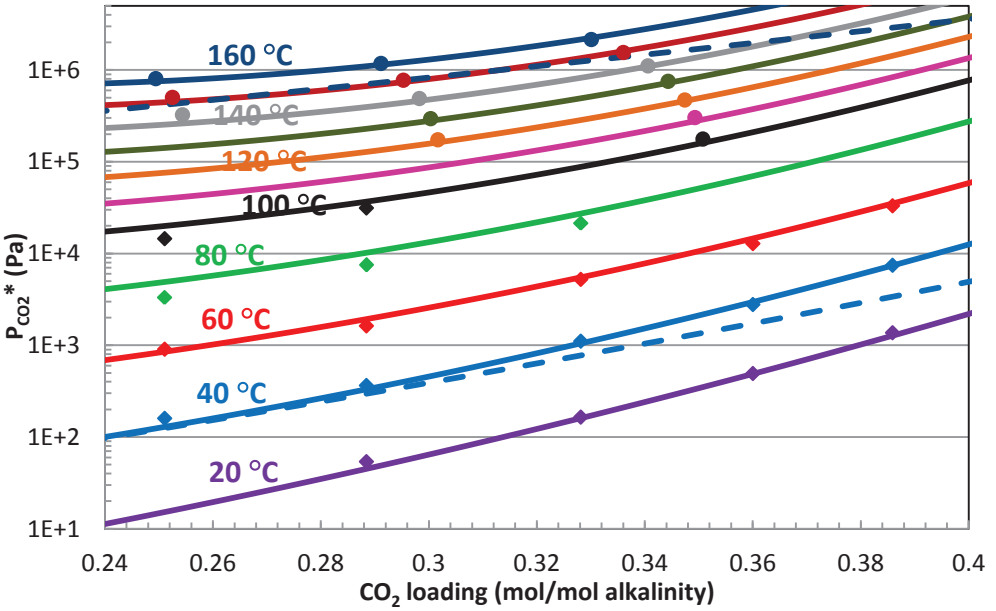

Figure 6: CO_2 solubility in 5 m PZ/2 m AEP. Diamonds: WWC results; Circles: total pressure results; Solid lines: model prediction (Equation 7); Dashed lines: model for 8 m PZ [4].

Table 2: Parameter values for the semi-empirical VLE model (Equation 7) for PZ blends

(m) PZ /(m) Am	a	b	c	d	e	f	R^2
6 / 2 HMDA	0	0	230 ± 8	-368 ± 21	-72489 ± 2900	130983 ± 7402	1.000
6 / 2 DAB	41.2 ± 4.1	-16399 ± 1231	-27.3 ± 10.4	0	30302 ± 4312	-16358 ± 6569	0.992
6 / 2 BAE	0	0	190 ± 7	-264 ± 18	-56669 ± 2386	91862 ± 6373	1.000
5 / 2 AEP	58.3 ± 12.3	-17587 ± 4184	-138 ± 81	200 ± 131	42830 ± 27306	-47262 ± 44107	0.998
5 / 2.3 AMP [b]	23. 9± 6.6	-6575 ± 2527	88.5 ± 35.6	-160 ± 47	-28165 ± 13518	60725 ± 17866	0.999
2 / 4 AMP [b]	31.4 ± 4.2	-8654 ± 1562	32.4 ± 23.1	-55.9 ± 30.9	-9562 ± 8362	22848 ± 10997	0.999
8 m PZ [a]	35.3 ± 0.3	-11054 ± 120	0	-18.9 ± 2.7	4958 ± 347	10163 ± 1085	0.993
7 m MEA [a]	38.6 ± 0.4	-12379 ± 139	0	-16 ± 2.5	3556 ± 231	8702 ± 932	0.994

[a] Ref [4].

[b] P_{CO2}* data in Ref [2]

For all four blends, the two sets of results by different experimental methods agree well with each other. The quality of regressed fit for the semi-empirical models is high for 6 m PZ/2 m HMDA, 6 m PZ/2 m BAE, and 5 m PZ/2 m AEP, with R^2 values close to one. The data for 6 m PZ/2 m DAB show significantly larger variations, particularly within the total pressure result (Figure 4). The R^2 of the regressed model for 6 m PZ/2 m DAB is slightly less than other blends, but still shows good predictability. Also, the VLE curves predicted by this model are physically reasonable within the range of the experimental conditions.

3.1.1. Capacity (ΔC_{solv})

Solvent capacity is the difference in CO_2 concentration between the lean and rich conditions. It can be calculated by Equation 8 and the VLE model (Table 2).

$$\Delta C_{solv} = \frac{(\propto_{rich} - \propto_{lean}) \cdot mol\ alkalinity}{kg\ (amine + H_2O)} = \frac{mol\ CO_2}{kg(amine + H_2O)} \quad (8)$$

ΔC_{solv} represents the amount of CO_2 removed per unit mass of solvent required. Solvents with higher ΔC_{solv} are more energy efficient because less of it is needed per mole of CO_2 removal. ΔC_{solv} depends on the difference between lean and rich loading ($\Delta\alpha_{CO2}$) and the concentration of total alkalinity. The $\Delta\alpha_{CO2}$ of a solvent depends on its CO_2 solubility at 40 °C; a large $\Delta\alpha_{CO2}$ corresponds to a flat VLE curve.

The 40 °C VLE curve for the blends is plotted in Figure 6, together with 5 m PZ/2.3 m AMP and 2 m PZ/4 m AMP, all compared against 8 m PZ, 7 m MEA, 6 m AEP, and 4.8 m AMP. The concentrated PZ blends have $\Delta\alpha_{CO2}$ slightly less than 8 m PZ. The primary diamine blends (HMDA, DAB, BAE) have higher lean and rich CO_2 loading than 8 m PZ, as a result of the high pKa for the primary amines. Since CO_2 solubility decreases with increased CO_2 loading, high pKa values contribute to reduced $\Delta\alpha_{CO2}$. The curve for PZ/AEP lies between 8 m PZ and 6 m AEP, and the reduced solubility of this blend is the result of the weak alkalinity by the tertiary nitrogen group in AEP. AMP, a hindered amine, has large $\Delta\alpha_{CO2}$ [7]. For PZ/AMP, the $\Delta\alpha_{CO2}$ increases with increased AMP in the blend, and both are higher than 8 m PZ. However, the ΔC_{solv} of PZ/AMP is less than 8 m PZ despite the higher $\Delta\alpha_{CO2}$ due to low concentration of alkalinity. The ΔC_{solv} for PZ/DAB, PZ/BAE, and PZ/AEP is about 20% lower than 8 m PZ but still about 15% higher than 7 m MEA. PZ/HMDA has low ΔC_{solv}, similar to that of 7 m MEA (Table 3).

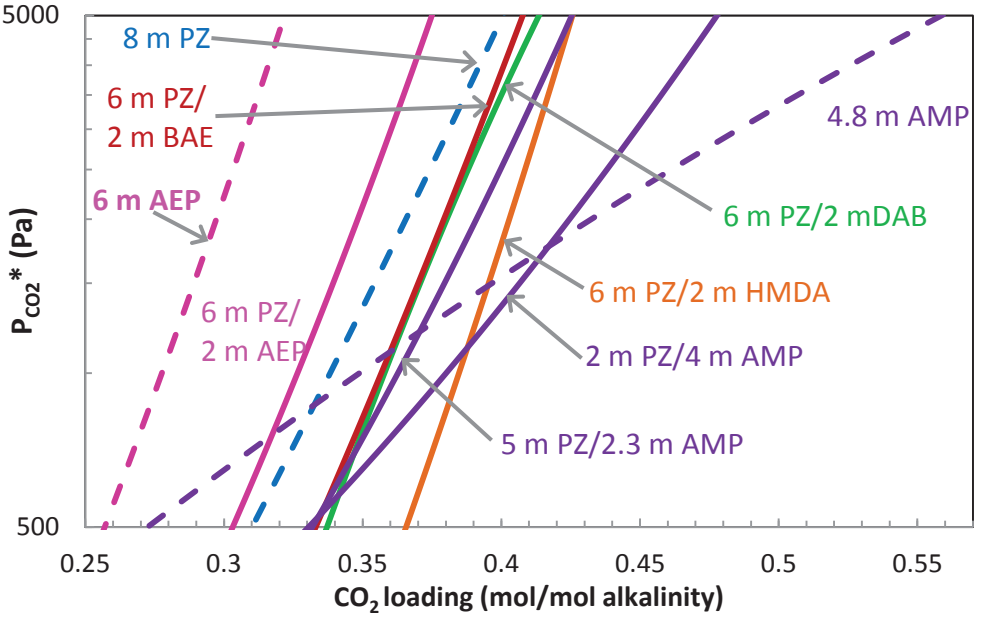

Figure 6: CO_2 solubility at 40 °C between lean and rich loading (P_{CO2}* 0.5-5 kPa) for PZ blends. Compared against dashed lines: 8 m PZ [4], 4.8 m AMP [7], 6 m AEP [8].

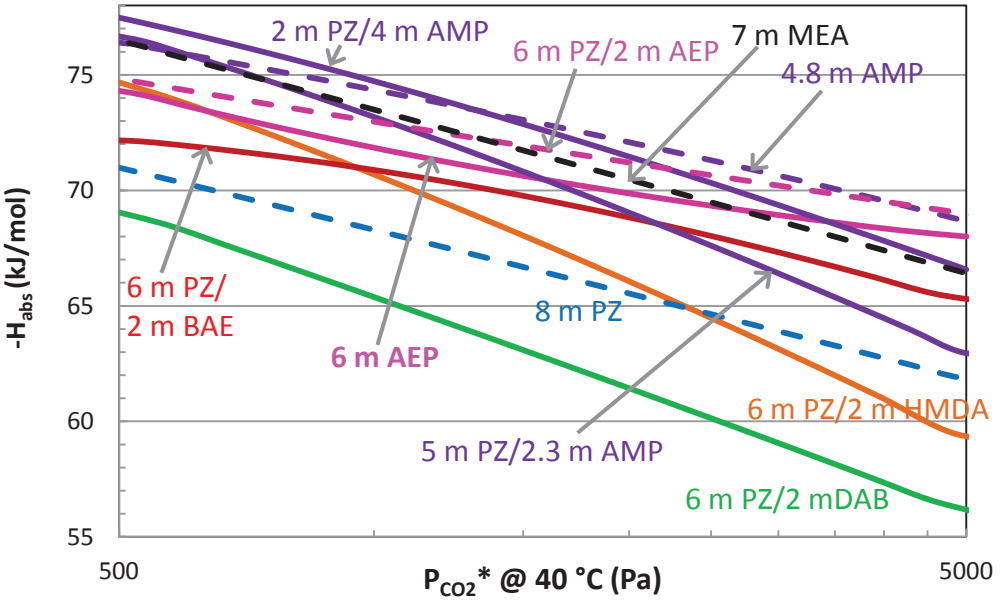

Figure 7: Heat of CO_2 absorption (Equation 9) between lean/rich loading (P_{CO2}* 0.5- 5 kPa at 40°C) for PZ blends. Compared against dashed lines: 8 m PZ, 7 m MEA [4], 4.8 m AMP [7], and 6 m AEP [8].

3.1.2. Heat of CO_2 absorption (ΔH_{abs})

The heat of CO_2 absorption in a solvent can be predicted from CO_2 solubility measurements. Theoretically, ΔH_{abs} is the temperature dependence of P_{CO2}* and can be calculated by taking the derivative of the semi-empirical VLE model (Equation 9).

$$-\Delta H_{abs} = R \cdot \left(\frac{\partial \ln (P^*_{CO_2})}{\partial (1/T)}\right)_{P,x} = b + e \cdot \alpha_{CO_2} + f \cdot {\alpha_{CO_2}}^2 \quad (9)$$

The mathematical expression shows, at conditions where the VLE model is valid, ΔH_{abs} is not a function of temperature but depends strongly on CO_2 loading. Previously modelling results show high ΔH_{abs} contributes to better energy performance in a process at constant stripper temperature [6].

The predicted ΔH_{abs} of the new PZ blends and the PZ/AMP are compared against 8 m PZ, 7 m MEA, 4.8 m AMP, and 6 m AEP between solvent lean and rich loading (Figure 7). At the same P_{CO2}*, ΔH_{abs} differs by less than 10 kJ/mol for all solvents. AMP, PZ/AMP, AEP, and PZ/AEP have high ΔH_{abs} compared to 7 m MEA. 6 m PZ/2 m BAE has intermediate ΔH_{abs} values, between 7 m MEA and 8 m PZ. ΔH_{abs} for 6 m PZ/2 m HMDA is high at lean loading but decreases significantly with increased loading. 6 m PZ/2 m DAB has lower ΔH_{abs} than 8 m PZ. While HMDA and DAB have high pKa values with high intrinsic ΔH_{abs}, they also contribute to high lean and rich loading of the blends. Since ΔH_{abs} decreases with increased loading, the practical ΔH_{abs} at the relevant loading range for PZ/HMDA and PZ/DAB is lower than expected. The predicted ΔH_{abs} at solvent lean loading and the mid-loading (P_{CO2}* 1.5 kPa) for the blends is summarized in Table 3.

3.1.3. Energy performance

The energy performance of a solvent depends on its ΔH_{abs} and the thermal stability of the amines. The rate of solvent degradation limits the temperature of the stripper. Measured rates of thermal degradation for the new PZ blends are used to predict the maximum stripper operating temperature (T_{max}) [1, 11, 12]. With the predicted T_{max}, the corresponding maximum stripper pressure (P_{max}) can be calculated [12]. Solvents with a combination of high T_{max} and ΔH_{abs} will also have high P_{max}. High P_{max} reduces the work required to compress the removed CO_2, and lowers the overall energy cost. The ratio of CO_2 and water vapor at the top of the stripper (P_{CO2}/P_{H2O}) also suggests relative energy performance of the solvent. With high CO_2 to H_2O ratio, less stripping steam is required per mole of CO_2 removed which means less total energy requirement. P_{CO2}/P_{H2O} also increases with an increase in ΔH_{abs} and T_{max}. Thus, 6 m PZ/2 m HMDA, 6 m PZ/2 m BAE, and 5 m PZ/2 m AEP, with both high Tmax and ΔH_{abs} are expected to have the best energy performance compared to the other blends and are competitive against 8 m PZ.

The cost associated with heating the solvent depends on ΔC_{solv} and solvent viscosity to the 0.25 power [12]. To demonstrate this effect of viscosity on the heat cost in the process, a new parameter is defined by normalizing solvent capacity by the viscosity of the loaded solvent (Equation 10).

$$\Delta C_\mu = \frac{\Delta C_{solv}}{\left({}^{\mu\alpha_{mid}}/_{10\ cP}\right)^{0.25}} [=] \frac{mol\ CO_2}{kg\ (H_2O + amine)} \quad (10)$$

The values of P_{max}, P_{CO2}/P_{H2O}, and the viscosity normalized solvent capacity (ΔC_μ) for the blends are summarized in Table 3.

Table 3: Summary of composition, absorption rate, and process performance of new PZ blends

PZ		Amine		Absorption rate		CO_2 solubility					Energy Performance			
				$k_g'_{avg}$ [a]	A_p/V_g [a]	$\alpha_{lean/rich}$	Capacity		- H_{abs}		T_{max} [c]	P_{max} [c]	$P_{CO2}/$ [c]	μ [d]
m	wt%	m	wt%		$x10^3$ s/m	mol/mol	ΔC_{solv}	ΔC_{μ}	mid [b]	lean	°C	bar	P_{H2O}	cP
6	0.30	HMDA (2)	0.13	4.9	3.1	0.37/0.43	0.55	0.49	68	75	161	20.1	2.61	15.4
6	0.31	DAB (2)	0.10	7.1	2.1	0.34/0.41	0.68	0.66	63	69	157	11.7	1.3	11.6
6	0.30	BAE (2)	0.12	7.3	2.1	0.33/0.41	0.69	0.66	70	72	157	14.2	1.8	11.7
5	0.26	AEP (2)	0.15	8.1	1.8	0.30/0.37	0.68	0.67	71	75	155	15.4	2.2	10.9
5	0.37	AMP (2.3) [e]	0.11	7.5	2.0	0.33/0.43	0.70	0.71	71	77	128	5.3	1.4	9.5
2	0.11	AMP (4) [e]	0.23	8.3	1.8	0.33/0.48	0.77	0.9	73	77	128	5.6	1.45	5.4
8	0.40	/		8.5	1.8	0.31/0.40	0.86	0.84	67	71	163	16.5	1.8	10.8
		MEA (7)	0.30	4.3	3.5	0.43/0.53	0.50	0.67	72	76	121	3.8	1.1	3

[a] Calculated for 90% CO_2 removal from coal by an isothermal absorber at 40 °C.

[b] Calculated at CO_2 loading with P_{CO2}* = 1.5 kPa

[c] Ref [12].

[d] Average viscosity between lean and rich loadings at 40 °C.

[e] Ref [2], [12]

3.2. Absorption rate

The k_g' for 6 m PZ/2 m HMDA, 6 m PZ/2 m DAB, 6 m PZ/2 m BAE, and 5 m PZ/2 m AEP is plotted against P_{CO2}* at 40 °C (Figures 8–11). P_{CO2}* at 40 °C is used in place of CO_2 loading to 1) more directly compare 40 °C results of different solvents at the same mass transfer driving force in an real absorber, and 2) conveniently compare k_g' at different temperature at the same CO_2 loading.

6 m PZ/2 m HMDA has a low absorption rate at 40 °C, which is only slightly higher than 7 m MEA at low loading and lower than MEA at high loading. The low rate of this blend is attributed to its high viscosity, which lowers the D_{CO2} in the liquid; at the same P_{CO2}*, the blend has higher loading than 8 m PZ, which corresponds to lower free amine for absorption (Equation 3). 6 m PZ/2 m DAB and 6 m PZ/2 m BAE have good rate at 40 °C, with k_g' slightly lower than 8 m PZ. With the three primary diamine blends (HMDA, DAB, BAE), k_g' decreases with increase in temperature. This dependence is more significant at high temperature and CO_2 loading. This temperature effect follows the same trend as the temperature dependence of viscosity and D_{CO2} (Equation 2), which suggests mass transfer in these blends is more dependent on diffusion. All three blends have high viscosity and relatively high rich and lean loading, both of which contribute to strong dependence of k_g' on diffusion. 5 m PZ/2 m AEP has competitive k_g' compared to 8 m PZ. For the PZ/AEP blend, k_g' changes little with change in temperature. The k_g' of the blend compared to 6 m AEP suggests the reacting species in the blend is mostly PZ species.

An average k_g' ($k_g'_{avg}$) can be calculated for a 40 °C isothermal absorber with 90% CO_2 removal from coal flue gas (Equation 11).

$$k'_{g\,avg} = \frac{Flux_{CO_2,LM}}{(P_{CO_2} - P^*_{CO_2})_{LM}} = \frac{(Flux_{CO_2,top} - Flux_{CO_2,bottom})/Ln(Flux_{CO_2,top}/Flux_{CO_2,bottom})}{(1.2kPa - 0.5kPa) - (12kPa - 5kPa)/Ln(\frac{1.2kPa - 0.5kPa}{12kPa - 5kPa})} \quad (11)$$

$k_g'_{avg}$ is calculated by assuming a linear concentration profile and equilibrium curve in the absorber. The packing area required per unit of flue gas that corresponds to $k_g'_{avg}$ can be calculated using Equation 12.

$$\frac{A_p}{V_g} = \frac{Removal \cdot x_{CO_2} \cdot P/RT}{Flux_{CO_2,LM}} = \frac{90\% \cdot 12\% \cdot P/RT}{k'_{g\,avg}(P_{CO_2} - P^*_{CO_2})_{LM}} \quad (12)$$

The $k_g'_{avg}$ and A_p/V_g for the PZ blends are summarized in Table 3.

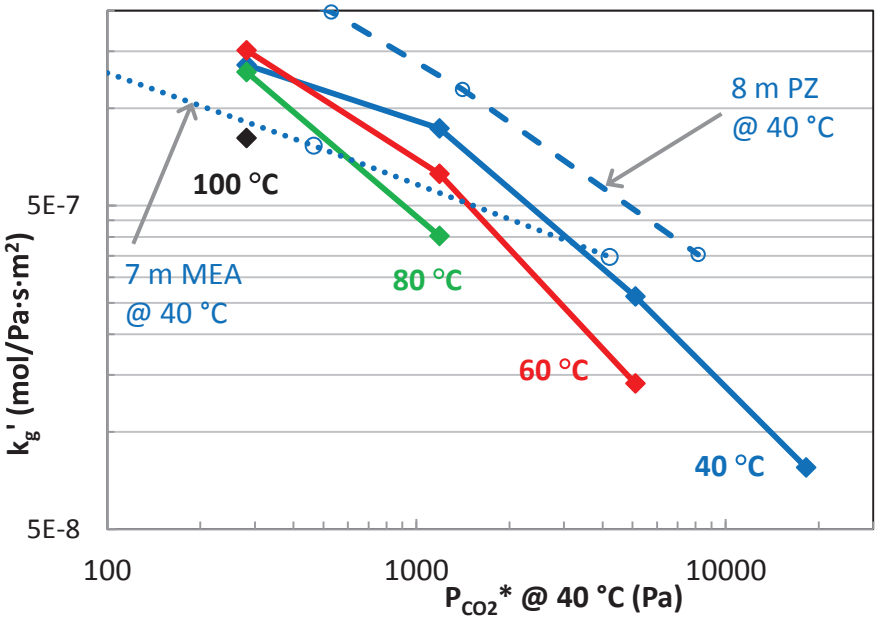

Figure 8: Absorption rate of 6 m PZ/2 m HMDA compared against dashed lines for 8 m PZ and 7 m MEA at 40 °C [3].

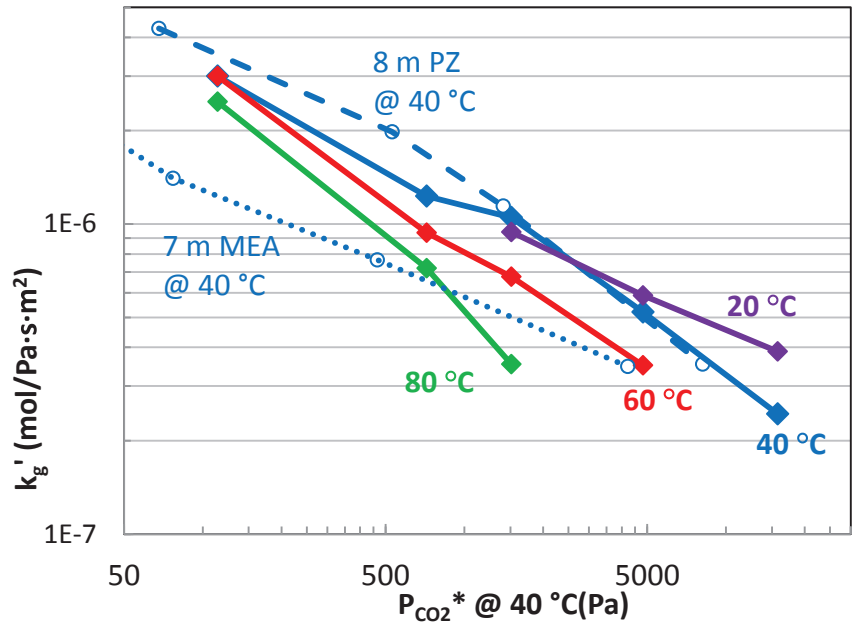

Figure 8: Absorption rate of 6 m PZ/2 m DAB compared against dashed lines for 8 m PZ and 7 m MEA at 40 °C [3].

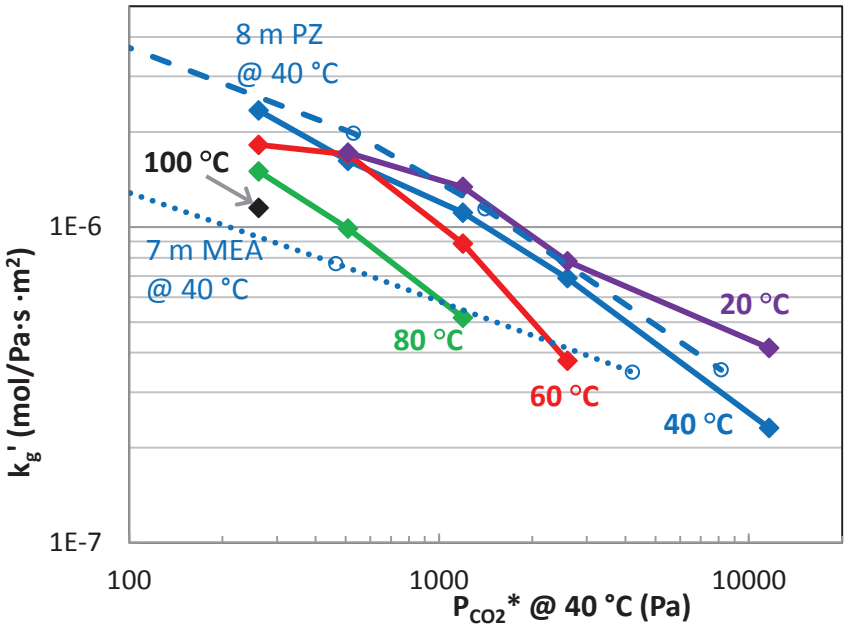

Figure 9: Absorption rate of 6 m PZ/2 m BAE compared against dashed lines for 8 m PZ and 7 m MEA at 40 °C [3].

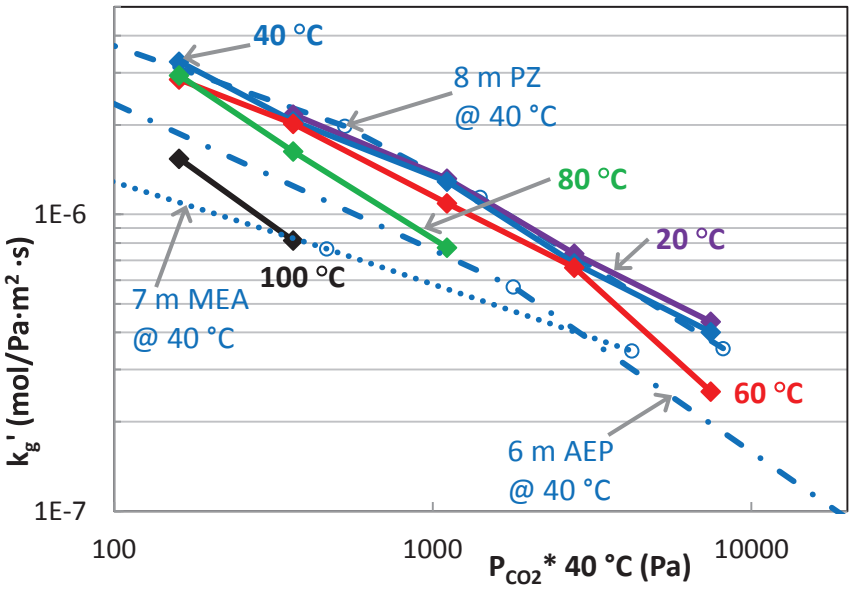

Figure 10: Absorption rate of 5 m PZ/2 m AEP compared against dashed lines for 8 m PZ, 7 m MEA [3], and 6 m AEP [8] at 40 °C.

Table 4: Measured k_g' and P_{CO2}* for 6 m PZ/2 m HMDA

WWC				Total pressure		
T °C	α_{CO2} mol/mol	P^*_{CO2} (kPa)	k_g' X10^7 (mol/s·Pa·m^2)	T °C	α_{CO2} mol/mol	P^*_{CO2} (kPa)
40	0.35	0.28	13.6	100	0.414	124
	0.40	1.19	8.7		0.414	125
	0.43	5.11	2.6	120	0.409	388
	0.46	18.2	0.78		0.409	382
60	0.35	1.82	15.1		0.345	101
	0.40	7.82	6.3		0.345	100
	0.43	28.7	1.4	140	0.398	925
80	0.35	9.18	12.9		0.398	919
	0.40	35.7	4.0		0.341	319
100	0.35	35.5	8.1		0.341	327
				160	0.381	1841
					0.330	861

Table 5: Measured k_g' and P_{CO2}* for 6 m PZ/2 m DAB

WWC				Total Pressure					
T °C	α_{CO2} mol/mol	P_{CO2}^* kPa	k_g' X10^7 (mol/s·Pa·m^2)	T °C	α_{CO2} mol/mol	P_{CO2}^* kPa	T °C	α_{CO2} mol/mol	P_{CO2}^* kPa
20	0.372	0.24	9.4	100	0.418	183	140	0.360	375
	0.398	0.64	5.9		0.459	214		0.366	314
	0.425	1.75	3.9		0.471	349		0.402	676
40	0.300	0.11	30.0	110	0.409	150		0.405	1198
	0.351	0.72	12.3		0.416	331		0.412	928
	0.372	1.51	10.5		0.421	236		0.443	1429
	0.398	3.57	5.2		0.456	449		0.453	1700
	0.425	11.66	2.4		0.467	603	150	0.357	656
60	0.300	0.92	30.0	120	0.408	249		0.398	1028
	0.351	4.55	9.4		0.413	521		0.363	551
	0.372	7.94	6.8		0.419	359		0.399	1703
	0.398	19.81	3.5		0.453	641		0.406	1343
80	0.300	3.68	24.8		0.464	853		0.436	1959
	0.351	19.77	7.2	130	0.363	199	160	0.352	1040
	0.372	37.21	3.5		0.367	210		0.392	1491
					0.406	434		0.359	874
					0.409	819		0.400	1881
					0.416	617			
					0.448	1025			
					0.458	1264			

Table 6: Measured k_g' and P_{CO2}* for 6 m PZ/2 m BAE

WWC				Total pressure		
T °C	α_{CO2} mol/mol	P_{CO2}* kPa	$k_g' \times 10^7$ (mol /s·Pa·m^2)	T °C	α_{CO2} mol/mol	P_{CO2}* kPa
20	0.333	0.07	17.2	100	0.396	169
	0.362	0.13	13.4		0.428	476
	0.392	0.39	7.8	110	0.394	320
	0.420	1.53	4.1		0.423	820
40	0.305	0.26	23.4	120	0.356	207
	0.333	0.51	16.2		0.392	518
	0.362	1.20	11.1		0.419	1099
	0.392	2.60	6.9	130	0.354	379
	0.420	11.6	2.3		0.388	827
60	0.305	1.51	18.2		0.412	1598
	0.333	2.48	17.0	140	0.338	372
	0.362	6.46	8.9		0.351	609
	0.392	16.2	3.8		0.383	1221
80	0.305	7.04	15.0		0.406	2077
	0.333	12.0	9.9	150	0.334	635
	0.362	28.0	5.2		0.346	955
100	0.305	27.2	11.5		0.377	1745
				160	0.330	995
					0.341	1418

Table 7: Measured k_g' and P_{CO2}* for 5 m PZ/2 m AEP

WWC				Total P		
T °C	α_{CO2} mol/mol	P_{CO2}* kPa	$k_g' \times 10^7$ (mol /s·Pa·m^2)	T °C	α_{CO2} mol/mol	P_{CO2}* kPa
20	0.288	0.05	21.7	100	0.351	177
	0.328	0.17	13.2	110	0.349	303
	0.360	0.49	7.38	120	0.302	174
	0.386	1.37	4.35		0.347	472
40	0.251	0.16	32.7	130	0.300	295
	0.288	0.37	20.6		0.344	753
	0.328	1.11	12.9	140	0.254	325
	0.360	2.78	6.84		0.298	489
	0.386	7.46	4.01		0.341	1110
60	0.251	0.91	28.5	150	0.253	503
	0.288	1.63	20.2		0.295	774
	0.328	5.23	10.9		0.336	1552
	0.360	12.8	6.62	160	0.249	806
	0.386	33.1	2.53		0.291	1180
80	0.251	3.33	29.4		0.330	2150
	0.288	7.54	16.3			
	0.328	21.4	7.73			
100	0.251	14.5	15.4			
	0.288	31.4	8.17			

4. Conclusions

- 6 m PZ/2 m HMDA, 6 m PZ/2 m DAB, and 6 m PZ/2 m BAE have ΔC_{solv} about 20% lower than 8 m PZ due to the high pKa of the primary diamines. 5 m PZ/2 m AEP have lower ΔC_{solv} than 8 m PZ due to reduced alkalinity of the tertiary nitrogen. The PZ/AMP blends have high $\Delta\alpha_{CO2}$ but lower ΔC_{solv} because of the low concentration of alkalinity in the blends.
- The ΔH_{abs} of 5 m PZ/2 m AEP and 2 m PZ/4 m AMP are competitive against 7 m MEA. 6 m PZ/2 m BAE and 6 m PZ/2 m HMDA have slightly higher ΔH_{abs} than 8 m PZ. The ΔH_{abs} for 6 m PZ/2 m DAB is lower than 8 m PZ. Overall, the difference in ΔH_{abs} among the blends is within 10 kJ/mol in the practical loading range.
- 6 m PZ/2 m HMDA, 6 m PZ/2 m BAE, and 5 m PZ/2 m AEP have good energy performance compared with 8 m PZ, because of the combination of high ΔH_{abs} and thermal stability.
- The absorption rate of 5 m PZ/2 m AEP is competitive with 8 m PZ at 40 °C. 6 m PZ/2 m DAB and 6 m PZ/2 m BAE have rates about 10% lower than 8 m PZ at 40 °C. 6 m PZ/2 m HMDA have low rates, similar to 7 m MEA, which is due to high solvent viscosity and high loadings. Mass transfer in the HMDA, DAB, and BAE blends is likely diffusion controlled.

5. Acknowledgements

The authors acknowledge the support of the Luminant Carbon Management Program.

6. References

[1] Namjoshi O, Du Y, Rochelle GT. Thermal degradation of piperazine blends with diamines. *Presented at GHGT-11, Kyoto, Japan, November 18-22, 2012. Energy Procedia, 2013.*
[2] Li H, Li L, Nguyen T, Rochelle GT, Chen J. Characterization of piperazine/2-aminomethylpropanol. Presented at GHGT-11, Kyoto, Japan, November 18-22, 2012. Energy Procedia, 2013.
[3] Dugas RE. *Carbon dioxide absorption, desorption, and diffusion in aqueous piperazine and monoethanolamine*. Ph.D. Dissertation, The University of Texas at Austin, Austin, Texas, 2009
[4] Xu Q. *Thermodynamics of CO_2 loaded aqueous amines*. The University of Texas at Austin, Austin, Texas, 2011.
[5] Rochelle GT, et al. Aqueous piperazine as the new standard for CO_2 capture technology. *Chemical Engineering Journal* 2011; 171:725-733.
[6] Oyenekan BA, Rochelle GT. Energy performance of stripper configurations for CO_2 capture by aqueous amines. *Industrial & Engineering Chemistry Research* 2006; 45(8): 2457-2464.
[7] Chen X, Closmann F, Rochelle GT. Accurate Screening of Amines by the Wetted Wall Column. *Energy Procedia*. 2011; 4: 101-108.
[8] Chen X, Rochelle GT. Aqueous Piperazine Derivatives for CO_2 Capture: Accurate Screening by a Wetted Wall Column. Chemical Engineering Research and Design 2011; 89(9):1693-1710.
[9] Bishnoi S, Rochelle GT. Absorption of carbon dioxide into aqueous piperazine: reaction kinetics, mass transfer and solubility. Chemical Engineering Science 2000; 55(22): 5531-5543.
[10] DIPPR, 1998-Provo, UT: BYU DIPPR, Thermophysical Properties Laboratory, 1998-Version 13.0.
[11] Freeman SA. *Thermal degradation and oxidation of aqueous piperazine for carbon dioxide capture.* PhD Dissertation, The University of Texas at Austin, Austin, Texas, 2010.
[12] Li L, et al. Amine blends using concentrated piperazine. *Presented at GHGT-11, Kyoto, Japan, November 18-22, 2012. Energy Procedia, 2013.*